Inter-Leaflet Phospholipid Exchange Impacts the Ligand Density Available for Protein Binding at Supported Lipid Bilayers

Grant J. Myres, Jay P. Kitt, and Joel M. Harris*
Department of Chemistry, University of Utah, 315 South 1400 East
Salt Lake City, UT 84112-0850 USA

Abstract

Phospholipid bilayers formed at solid-liquid interfaces have garnered interest as mimics of cell-membranes to model association reactions of proteins with lipid-bilayer-tethered ligands. Despite the importance of understanding how ligand density in a lipid bilayer impacts the protein-ligand association response, relating the ligand-modified lipid fraction to the absolute density of solution-accessible ligands in a lipid bilayer remains a challenge in interfacial quantitative analysis. In this work, confocal-Raman microscopy is employed to quantify the association of anti-biotin IgG with a small fraction of biotinylated lipids dispersed in either gel-phase or liquid-crystalline supported lipid bilayers, deposited on the interior surfaces of wide-pore silica surfaces. We examine the question whether inter-leaflet lipid translocation contributes to the population of solution-accessible biotin ligands on the distal leaflet of a supported lipid bilayer by comparing their protein accumulation response with ligands dispersed in lipid monolayers on nitrile-derivatized silica surfaces. The binding of antibody to biotin ligands dispersed in gel-phase bilayers exhibited an equivalent biotin-coverage response as the accumulation of IgG onto gel-phase monolayers, indicating that gel-phase bilayer symmetry was preserved. This result contrasts with the ~60% greater anti-biotin capture observed at fluid-phase bilayers compared to fluid-phase monolayers prepared at equivalent biotin fractions. This enhanced protein capture is attributed to biotin-capped lipids being transferred from the surface-associated proximal leaflet of the bilayer to the solution-exposed distal leaflet by the inter-leaflet exchange or lipid flip-flop, a facile process in fluid-phase supported lipid bilayers. The results suggest caution in interpreting the results of quantitative studies of protein binding to lipid-tethered ligands dispersed in fluid-phase phospholipid bilayers.

***** Corresponding author: harrisj@chem.utah.edu

INTRODUCTION

Supported lipid bilayers on planar glass supports are attractive interfaces for biosensing applications given their ease of assembly at solid/liquid interfaces by vesicle fusion[1,2] and generally low affinities for non-specific interactions with biomolecules.[3] Lipid bilayers formed on solid supports have also been used as models of cell membranes to investigate interfacial biorecognition between proteins in solution and their corresponding lipid-bound ligands.[4-6] These applications of supported lipid bilayers have shown that lipid-bilayer structure and dynamics, including lateral mobility,[7-9] density,[10-12] and accessibility,[10,13] play a role in governing protein-binding affinity, producing results that differ from protein-association reactions with ligands that are tethered at fixed locations on a solid surface.[9,14,15]

A dynamic process observed in supported lipid bilayers that could impact protein-ligand binding at lipid bilayer interfaces is the exchange of lipids between the two leaflets of the bilayer. Lipid leaflet-exchange has been reported to be fast in supported bilayers[16,17] where the rate of exchange is sensitive to temperature, lipid phase, and the head-group composition of the phospholipid, including size, hydration, and charge.[16-19] In addition, interactions of the lipid head-groups with the underlying support surface or with species in the overlaying solution have been shown to be capable of inducing bilayer asymmetry.[20-23] Compositional asymmetry in the two leaflets could result in either enhanced or inhibited accessibility of ligands at the solution-accessible outer-leaflet of the bilayer. Thus, for analysis of protein-ligand association, it is essential to understand the structure, dynamics, and possible asymmetry of the lipid bilayers and their influence on accessible ligand densities for protein binding.

Another challenge in quantitative analysis of protein-ligand binding at a lipid bilayer/solution interface is knowing the surface concentrations of both ligands and captured proteins. Several optical methods have been used to characterize protein binding to ligands tethered to planar-supported lipid bilayers, including fluorescence emission from labeled proteins,[24-27] surface plasmon resonance,[28-30] pH sensitive dyes,[31] and second harmonic generation.[32] These methods produce responses that are proportional to the population of captured protein and are useful for measuring binding isotherms. The protein surface coverages, however, are not generally measured but are estimated at the maximum response as a close-packed monolayer based on the size of the protein determined by crystallography.[33,34] The use of crystal structure data to estimate a maximum protein surface density neglects possible changes in protein

tertiary structure when the protein is bound to a ligand at a solution-bilayer interface compared to its conformation and size within a solid crystal.

It has been recently shown that phospholipid bilayers deposited by vesicle fusion on the interior surfaces of wide-pore (30- or 100-nm diameter) chromatographic silica particles can be characterized *in-situ* within individual particles with confocal Raman microscopy.[35] The high specific surface area of these porous silica supports provides a sufficient population of lipid molecules to overcome the sensitivity limitations of Raman scattering and allow facile detection of supported phospholipid bilayers. The large internal surface area of these particles also allows the lipid surface density to be determined by simple elemental (carbon) analysis of a small sample of material. From these results, the structure of these porous silica-supported lipid bilayers (head-group spacing, lipid bilayer thickness, and melting phase transition) were found to be comparable to supported bilayers formed on planar-surfaces.[35,36] Raman scattering from these bilayers has also been used to quantify the association response of a lectin protein, concanavalin A, with mannose-capped phospholipids incorporated into the porous-silica-supported lipid bilayers.[6] This study demonstrated that confocal Raman microscopy of ligand-modified phospholipid bilayers in high surface-area support particles can be an effective method for *in situ*, label-free, and quantitative investigation of protein-ligand interactions at supported lipid bilayer-solution interfaces.

In the present work, we employ this methodology to investigate the role that lipid bilayer leaflet exchange may play in the available lipid-tethered ligands that can react with proteins in solution. We also test whether lipid phase (gel versus liquid-crystalline) influences differences in solution-accessible ligand populations in bilayers that otherwise have an equivalent fraction of ligand-modified lipid. Specifically, we employ confocal Raman microscopy to measure the association of unlabeled anti-biotin IgG with biotin-capped lipid that is diluted into gel-phase and fluid phase supported-lipid bilayers and monolayers deposited onto the interior surfaces of wide-pore silica supports. Quantitative information on the surface coverages of both deposited lipids and captured antibody is acquired by *in situ* Raman scattering measurements within individual silica particles, calibrated *ex situ* by elemental carbon analysis of samples of the porous material. Using these methods, the surface densities of the deposited lipid bilayers and monolayers are compared to the densities of captured antibody to determine the distal-leaflet solution accessibility of the lipid-tethered biotin and its efficiencies for antibody binding.

EXPERIMENTAL SECTION

Reagents and materials. Spherical chromatographic silica particles were Sil-100nm-S-5μm from YMC America (Allentown, PA); for the particular sample lot, an average particle diameter D50 = 3.8 μm, uniformity D10/D90 = 1.43, and pore diameter of 110 nm were reported by the manufacturer. SEM images of the silica particles were acquired to reveal their pore structure which shows uniform 100-nm scale roughness throughout the regions of the particle that can be observed in these images (see Supporting Information, Figure S1). Water used in all experiments was filtered using a Barnstead GenPure UV water purification system (ThermoFisher Scientific, Waltham, MA) and had a minimum resistivity of 18.0 MΩ·cm. All phospholipids, 1-palmitoyl-2-oleoyl-*sn*-glycero-3-phosphocholine (POPC) and 1,2-dipalmitoyl-*sn*-glycero-3-phosphocholine (DPPC) from Avanti Polar Lipids, Inc. (Albaster, AL), and biotin-functionalized DPPE (1,2-dipalmitoyl-*sn*-glycero-3-PE-N-(cap biotin), sodium salt) from Cayman Chemical (Ann Arbor, Michigan), were dissolved in chloroform, and stored at -15°C until use. Monoclonal mouse anti-biotin IgG was purchased from Jackson ImmunoResearch Laboratories, Inc (West Grove, Pa) and stored at 2°C. Chloroform, sodium chloride, potassium chloride, potassium phosphate monobasic (KH_2PO_4), sodium phosphate dibasic heptahydrate ($Na_2HPO_4 \cdot 7H_2O$) were all purchased from Sigma-Aldrich (St. Louis, MO); (3-cyanopropyl)dimethylchlorosilane was purchased from Gelest (Morrisville, PA). To modify silica surfaces with nitrile groups for lipid-monolayer experiments,[36] 110-nm pore-diameter 4-μm silica particles were reacted with (3-cyanopropyl)-dimethyl-chlorosilane, details of which are in Supporting Information. The resulting surface coverage by nitrile groups was determined to be 2.5 ± 0.3 μmol/m^2 by comparison of the Raman scattering intensity from the -C≡N stretching mode of this nitrile-derivatized silica with a commercial nitrile-silica of known surface coverage; see Supporting Information.

Preparation of within-particle lipid bilayers and monolayers. To assemble supported lipid bilayers on the interior surfaces of wide-pore silica, the particles were first cleaned with acid piranha solution (60/40 concentrated sulfuric acid/30% hydrogen peroxide; *caution*: acid-piranha solutions are strongly oxidizing and can react explosively with organic compounds) followed by a triplicate rinsing in deionized water. Note that the acid-wash does not detectably affect the porous silica structure (Supporting Information). Dry lipid films of known composition were prepared by combining aliquots of chloroform-dissolved lipids (measured by mass on an analytical balance to avoid pipetting errors due to the high vapor pressure of chloroform) and drying the sample under flow of dry nitrogen. Complete evaporation of the solvent was achieved by a further drying step

under vacuum. Lipid vesicle dispersions were prepared at a concentration of 2 mg/ml from the dry lipid film by addition of pH 7.4 phosphate buffered saline (PBS) buffer and bath sonication at a temperature above the melting transition of the phospholipid to form small (<30 nm diameter) vesicles.[37] To deposit lipid bilayers within particles, sonicated vesicles were equilibrated with 1 mg/mL of cleaned porous silica in a stirring solution above the phospholipid melting temperature for ~12 hours. To ensure consistent bilayer coverages, a 25-fold excess of solution-phase lipid was used to limit any impacts on formation resulting from solution depletion. Following lipid vesicle fusion, particles were washed three times with PBS buffer and separated by centrifugation, where excess lipid was removed by drawing off the supernatant and re-suspending the particles in clean PBS buffer. Formation of lipid monolayers on the nitrile-modified silica particles was carried out via the same assembly procedure without acid-piranha cleaning (used only on the bare silica before the particles were nitrile-modified). The lipid concentration in the vesicle dispersion was decreased to 1 mg/mL to maintain the same ratio of solution-phase to surface-associated lipid.

Reactions of membrane-localized biotin ligands with anti-biotin IgG. Reactions of the biotin-ligands in porous-silica supported lipid bilayers and monolayers with solution-phase anti-biotin IgG were carried out as follows. A 1-μL aliquot of freshly prepared particles (1 mg/ml) was diluted into 99 μL of 300-nM anti-biotin IgG solution. The solutions contained more than a 50-fold excess of anti-biotin IgG compared to the within-particle biotin in the sample to avoid solution depletion of the antibody. The 300-nM solution concentration of IgG is 10-fold greater than the anti-biotin IgG:biotin dissociation constant,[10] thereby ensuring that the biotin ligands at the solution/bilayer or monolayer interface are saturated with bound antibody. To determine the absolute surface coverages of POPC supported-lipid bilayers and the saturation coverage of captured anti-biotin IgG, samples of the respective particles were washed multiple times with deionized water, dried under vacuum and submitted for carbon analysis at Midwest Laboratories (Indianapolis, IN). No loss of lipid or protein was detected as a result of the washing procedures (see Supporting Information).

Confocal Raman Microscopy. The confocal Raman microscope utilized has been previously described in detail elsewhere.[38] Briefly, the 647.1 nm emission band beam from a Kr^+ laser (Innova 90, Coherent Int., Sanata Clara, CA) was first passed through a narrow band pass filter followed by a 4X beam expander (50-25-4x-647, Special Optics Inc., Wharton, NJ), reflected off of a dichroic mirror, and directed to a 1.4 NA, 100X oil-immersion objective (CFL PLAN APO, Nikon Inc., El Segundo, CA) which produces a ~600-nm diameter beam waist at the focal

plane. Light scattered from the confocal probe volume was collected by the same objective, transmitted through the dichroic mirror, passed through a 660-nm long-pass filter and directed through the 50-μm wide entrance slit of a 0.5-m spectrograph (500 IS, Bruker Corp., Billerica, MA), where it was dispersed by a 300 lines/mm diffraction grating blazed at 750 nm, and refocused onto a charged coupled device (CCD) detector (Andor iDus 401A, Andor USA, South Windsor, CT).

To collect spectra, the laser beam was initially focused at the coverslip/solution interface and translated upward in the +Z direction until the perimeters of the silica particles resting on the coverslip surface were in sharp focus. The stage was then positioned in the x and y dimensions until the focused laser spot was centered within an individual particle. The resulting confocal detection volume centered in the particle, defined by the product of excitation beam profile and the confocal collection efficiency,[39] is illustrated in Supporting Information, Figure S5, where more than 95% of the collected scattering is from inside the particle. Raman spectra thus collected were truncated to the spectral region of interest and baseline corrected with rolling-circle algorithm.[40] All data analysis was conducted in Matlab (Mathworks, Natick, MA) using custom scripts. Well cells used in spectroscopic experiments were constructed by adhering a ~12-mm length of 10-mm i.d., 13-mm o.d. Pyrex glass tubing to No. 1 glass coverslip using Devcon 5 min epoxy (ITW Devcon, Danvers, MA).

RESULTS AND DISCUSSION

Formation and characterization of supported lipid bilayers and monolayers. DPPC and POPC supported-lipid bilayers were deposited onto the interior surfaces of 110-nm pore-diameter porous silica particles by fusion of sonicated vesicles in dispersion, at temperatures above their respective melting transition for 12 hours. Following lipid deposition, excess vesicles were removed by a buffer exchange and centrifugation; the resulting supported lipid bilayers were characterized by confocal Raman microscopy. Raman bands associated with phospholipid are highlighted in Figure 1 and assigned as follows:[35,41-45] the choline head-group symmetric stretching frequency is the same for both lipids, 720 cm^{-1}. For POPC and DPPC, the out-of-phase trans conformer C-C stretching modes appear at 1064 and 1067 cm^{-1}, while the in-phase trans conformer C-C stretch is at 1125 and 1130 cm^{-1}, respectively. The gauche conformer C-C stretching frequencies are 1086 and 1100 cm^{-1}, the CH_2 twisting mode appears at 1300 and 1295 cm^{-1}, and the CH_2 bending frequencies are 1442 and 1438 cm^{-1}, respectively. The C=C stretching mode from the double bond in the oleoyl chain of the POPC bilayer appears at 1655 cm^{-1}. The significantly

greater acyl-chain ordering of gel-phase DPPC compared to the fluid-phase POPC bilayer is apparent in the strong intensities of the out-of-phase and in-phase C-C stretching modes of the DPPC trans-conformer acyl-chains at 1064 cm^{-1} and 1130 cm^{-1}, respectively, compared to the gauche-conformer C-C stretching intensity at 1100 cm^{-1}.[45] Despite the significant laser power in the sample (130 mW), the consistent scattering from the trans-conformer modes of DPPC indicate that the monolayer and bilayer of this saturated lipid remain fully gel-phase throughout these experiments.

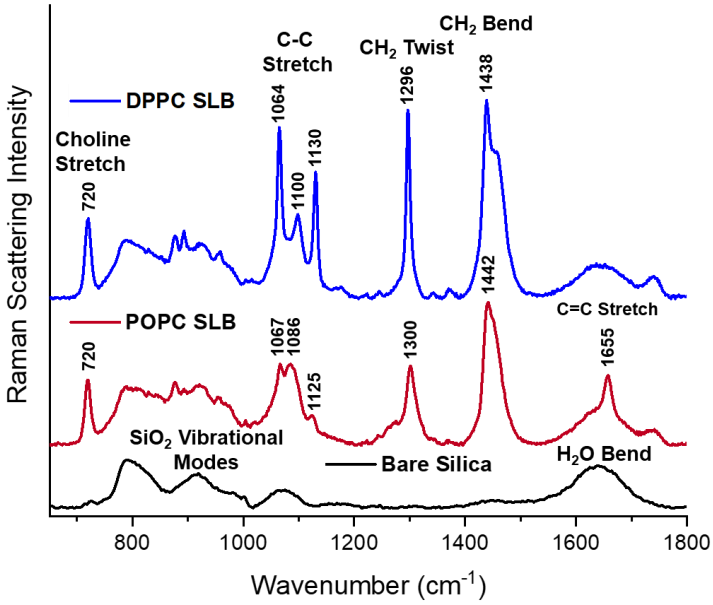

Figure 1. Formation of POPC and DPPC supported lipid bilayers (SLB) on 100-nm pore diameter silica particles. Raman spectra of bare silica (black), POPC supported lipid bilayer (red), and DPPC supported lipid bilayer (blue).

DPPC and POPC were deposited onto nitrile-derivatized (Supporting Information) porous silica surfaces using the same procedure. Comparison of the Raman scattering from nitrile-derivatized silica particles before and after lipid deposition reveals scattering from phospholipid and nitrile vibrational modes (Supporting Information, Figures S6 and S7). These data reveal a 4-cm^{-1} shift of the -C≡N mode to lower vibrational frequency upon accumulation of lipid (see inserts in Figures S6 and S7). This shift to lower frequency is consistent with a change in the interfacial environment from the high-dielectric constant of an aqueous solution to a low-dielectric constant environment, equivalent to a nitrile group in a hydrocarbon environment.[36,46] This result provides evidence that the surface-nitrile groups are in contact with the acyl-chains of the adsorbed lipid,[36] in agreement with the *tails-down monolayer structure* proposed for lipid monolayers on the surfaces of nitrile-derivatized glass nanopores.[47,48]

Further evidence for DPPC and POPC forming supported lipid monolayers on the nitrile-derivatized silica is provided by the Raman scattering intensities from accumulated phospholipids on bare versus nitrile-derivatized silica surfaces. Accounting for the small (~4%) difference in surface area of the two leaflets due to curvature of the pores,[35] one would anticipate that a supported-lipid bilayer on the same 110-nm porous-silica support would contain 1.96-times more phospholipid compared to a supported-lipid monolayer. We compare the Raman spectra from

POPC and DPPC deposited on bare and nitrile-terminated silica in Figure 2, where the total Raman scattering POPC deposited on bare silica exhibits 1.92 (±0.22) times greater intensity than POPC deposited on the nitrile-terminated surface. Similarly, DPPC deposited on bare silica produces 1.89 (±0.09) times greater intensity than DPPC on the nitrile surface (Figure 2). These quantitative results support the conclusion that POPC and DPPC deposited on the nitrile-terminated silica form phospholipid monolayers, where the nitrile-frequency response is consistent with lipid acyl-chains oriented towards the nitrile interface.[36,47]

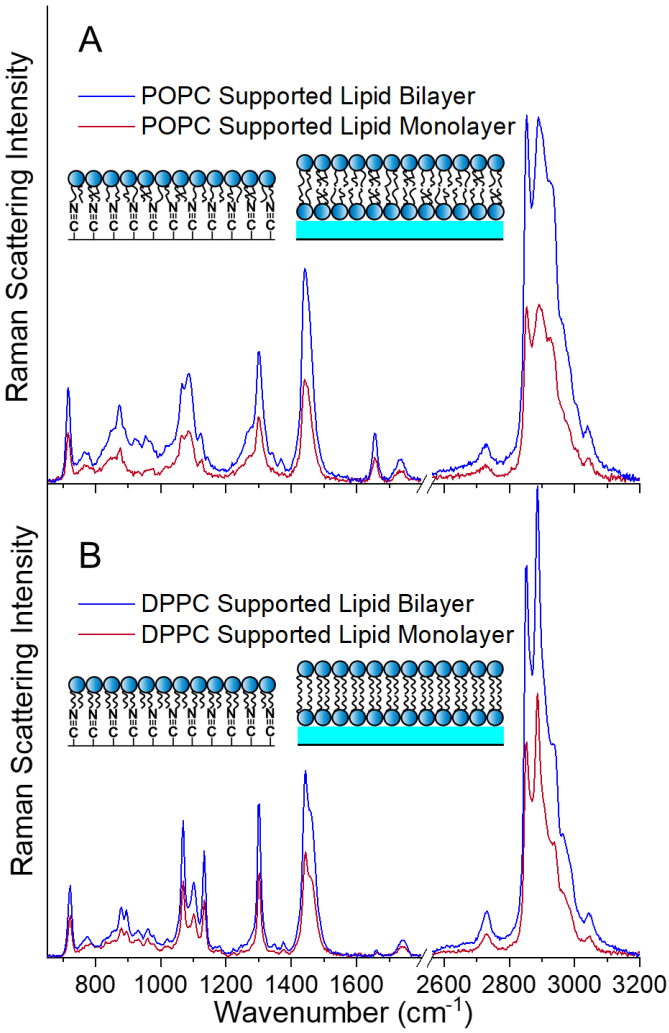

Figure 2. Comparison of Raman scattering intensities of phospholipids deposited as bilayers on bare porous silica (blue) and as monolayers on nitrile-derivatized silica (red) for (A) POPC and (B) DPPC, respectively.

Quantitative determination of lipid densities of supported bilayers and monolayers. The high specific surface area of the porous silica particles allows a small (10 mg) sample of particles to contain sufficient carbon in a lipid bilayer or monolayer to be quantified by elemental carbon analysis.[35,36,49] Using the specific surface area provided by nitrogen BET analysis and the carbon-mass% from elemental analysis, the *absolute* surface coverages of phospholipid can be determined.[35,36,49] The elemental carbon fraction of a POPC bilayer formed on bare porous silica particles was found to be 5.0 ±0.1%, corresponding to a total lipid coverage of POPC in the bilayer of 3.8 ±0.4 μmol/m^2 (Supporting Information). Correcting for the small (~4%) difference in surface area of the two leaflets due to curvature of the pores,[35] the total lipid in the bilayer corresponds to a solution-exposed distal-leaflet lipid surface density of 1.94 ±0.2 μmol/m^2 or an average head-group area of 84 ±9 Å^2. This result is ~15% greater than the 72.2 Å^2 head-group area of a 1,2-dioleoyl-sn-glycero-3-phosphocholine (DOPC) in a vesicle bilayer measured by x-ray diffraction[50] and may reflect small differences in packing of the lipid on the silica surface.

Using the carbon analysis results for the POPC lipid bilayer coverage as a standard, we quantify the POPC monolayer coverage on the nitrile surface by comparing the unnormalized Raman scattering intensities of the phospholipid bilayer on bare silica to the POPC monolayer on nitrile-derivatized silica (Figure 2A). We detect 52 ±6 % less total phospholipid intensity in the POPC monolayer compared to the POPC bilayer, which indicates a POPC surface density in the monolayer of 2.0 ± 0.2 μmol/m^2 or a head-group area of 83 ±8 Å^2, which is equivalent to the solution-exposed distal-leaflet density of the POPC silica-supported bilayer above. To determine the surface density of the DPPC monolayer on the nitrile surface, we use the scattering intensity of the -C≡N nitrile stretching mode as internal standard to normalize the POPC and DPPC nitrile-supported lipid Raman spectra and thereby quantify the surface coverages based on the relative intensities of the C-N choline stretching mode of the lipid (Supporting Information). The choline stretch is suitable for quantification because, unlike other phospholipid vibrational modes, its conformation is independent of phospholipid phase, leading to a consistent scattering cross-section.[51] This *in-situ* quantification shows 28 ± 2% more phospholipid is present in the DPPC monolayer compared to the POPC monolayer (Supporting Information). The resulting surface density of DPPC in the supported monolayer is 2.6 ± 0.2 μmol/m^2, corresponding to a lipid head-group area of 64 ±5 Å^2. This DPPC head-group area is in agreement with the 64 ±1 Å^2 head-group area of fluid-phase DPPC vesicle bilayers, determined by x-ray diffraction and neutron scattering at 50°C.[52,53] While the temperature at which the vesicle DPPC head-group area was measured is greater than for these Raman spectroscopy experiments, it is a relevant comparison because the DPPC monolayer surface density was established during its assembly on the nitrile surface under *fluid-phase conditions at ~50°C*. Finally, the surface density of the DPPC bare-silica-supported bilayer was determined by a comparison of its Raman spectrum with a DPPC monolayer (Figure 2B). The silica-supported DPPC bilayer exhibits 1.89±0.09-times greater total Raman scattering intensity than the nitrile-supported monolayer, where the total DPPC lipid density in the bilayer is 4.7 ±0.4 μmol/m^2. Corrected for the small (4%) difference in surface area of the two leaflets due to curvature of the pores, the total lipid corresponds to a solution-exposed distal-leaflet lipid surface density of 2.4 ±0.2 μmol/m^2 or a head-group area of 68 ±6 Å^2. This result is equivalent within measurement uncertainty to the nitrile-silica-supported DPPC monolayer and in agreement with head-group area of a DPPC vesicle bilayer at 50°C (see above).[52,53]

Detecting and quantifying the coverage of IgG bound to lipid-tethered ligands. The deposition of both DPPC and POPC lipids on the internal surfaces of bare- and nitrile-modified

silica particles produced structures that were consistent with supported lipid bilayers and monolayers, respectively. To detect and quantify the capture of anti-biotin IgG, a lipid bilayer was prepared as above on bare silica particles with POPC vesicles containing 5-mol% biotin-conjugated DPPE. A 1-µL aliquot of these particles (1 mg/ml) was diluted and mixed into 99-µL of 300-nM IgG in buffer. The 300-nM solution contains more than 50-fold excess of IgG relative to the within-particle biotin in the sample, substantially limiting any impact of solution-depletion on the measurement and the solution concentration of 300-nM IgG is 10-fold greater than the reported anti-biotin IgG:biotin dissociation constant,[10] ensuring that the biotin ligands available at the solution/bilayer or monolayer interface are saturated with bound antibody. Particles equilibrated with 300-nM anti-biotin IgG solution for ~5 hours were then washed three times with PBS buffer to remove excess protein. The Raman spectrum of the resulting sample is compared to a spectrum of the original 5% biotin-DPPE in POPC bilayer in Figure 3 and shows new vibrational features associated with the capture of the antibody. Subtracting the spectrum of the biotin-DPPE-POPC bilayer provides definitive evidence of antibody capture, producing a spectrum that is indistinguishable from a spectrum of anti-biotin IgG in 110-µM free solution (Figure 3(top)). The vibrational modes from Raman scattering of the captured protein are also identified in Figure 3.[6,54]

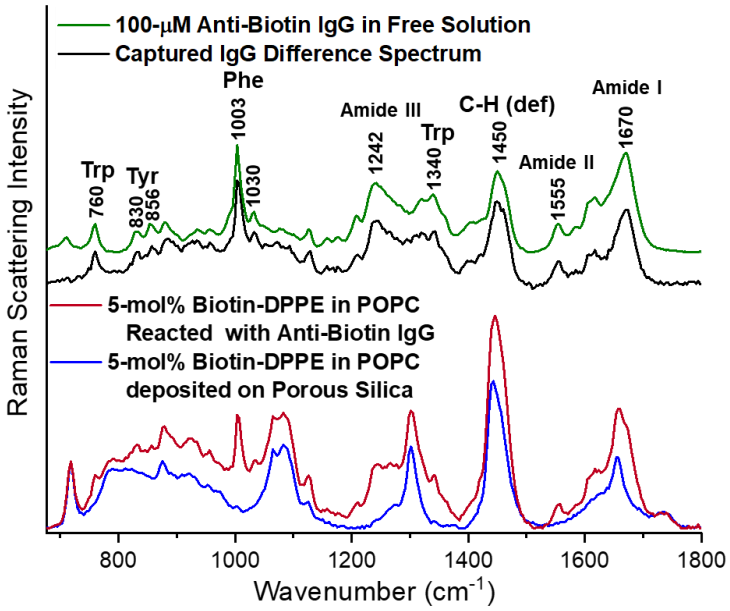

Figure 3. Capture of anti-biotin IgG at POPC bilayers prepared with 5-mol% biotin capped-DPPE. Below: Raman spectrum of silica-supported lipid bilayer prior (blue) is compared with the same bilayer following equilibration with 300-nM IgG (red). The difference spectrum above (black) provides evidence of antibody capture when compared to a spectrum of 100-µM anti-biotin IgG in free solution (green).

To ensure that the captured antibody shown in Figure 3 arises from specific interactions with the 5% biotin ligand in the lipid bilayer, a control experiment was carried out in which 1-µM anti-biotin IgG (3.3-times greater concentration than in the biotin-binding experiment in Figure 3) was equilibrated with a pure POPC lipid bilayer containing no biotin-DPPE. The difference spectrum in Supporting Information, Figure S9, shows no detectable protein bands arising from

non-specific adsorption of the antibody. Similar control experiments were carried out for POPC and DPPC lipid bilayers and monolayers, where no Raman scattering from non-specifically adsorbed anti-biotin IgG were detected (Figures S10-S12).

Having established the specificity of anti-biotin IgG binding, we next quantify the absolute surface density of bound protein. Typical optical methods for measuring interfacial protein-ligand binding do not report quantitative surface densities of protein-ligand complexes. Instead, the maximum coverage is estimated by assuming a close-packed protein array[5,24] where the intermolecular packing distances are estimated from x-ray crystallography data.[33,34] However, proteins immobilized at lipid membranes are solvated and dynamic, and their spacing at such interfaces could differ significantly from their structure in a crystalline solid. This issue is has been addressed in scanned probe microscopy measurements[55-58] of individual IgG molecules captured on a surface, which report molecular sizes consistently larger than values obtained by x-ray crystallography. These differences have been attributed to solvation,[57] which along with steric interactions can play a role in establishing the maximum coverage of a monolayer of surface-associated proteins.

Given the uncertainties in the structure and size of interfacial protein-ligand complexes, a far more reliable determination of their maximum surface density can be obtained through an *ex situ* analysis of the protein coverage of a macro-scale sample. To accomplish this goal, we again take advantage of the surface area of the porous silica supports that capture a sufficient quantity of interfacial protein that carbon analysis can be used to determine the maximum protein coverage on the equilibrated particles. POPC silica particles prepared with 5-mol% biotin-DPPE (a biotin-modified lipid fraction that produces a maximum IgG surface density, see below) were equilibrated with 300-nM anti-biotin IgG. The resulting particles were washed with buffer multiple times to remove the excess solution-phase IgG. The buffer-washed sample was then washed with DI water (to remove buffer components that would contribute to sample mass) and dried under vacuum for elemental carbon analysis. It is critical that no biotin-bound antibody is lost from the sample during these sample preparation steps. Therefore, the reversibility of the association between anti-biotin IgG with lipid-tethered biotin was tested on the time-scale of these experiments by preparing a sample of particles as above and then washing and storing the sample in excess buffer for 24 hours; the sample stored in buffer showed no detectable loss of bound antibody (Figure S13). Finally, the DI washing and vacuum drying steps were also tested and no loss of bound antibody was detected (Figure S14).

Elemental analysis of the particle sample prepared with a POPC bilayer containing 5-mol% biotin-DPPE and equilibrated with anti-biotin IgG resulted in a carbon mass fraction of 9.2 ± 0.6%. Subtracting the carbon fraction of particles with POPC and 5-mol% biotin-DPPE (5.4 ± 0.1%) showed an increase of 3.8 ± 0.6% in carbon mass fraction from the binding of the anti-biotin IgG. Using the carbon molecular weight of a mouse-derived monoclonal antibody[59] and the specific surface area of the silica, this increase in carbon mass corresponds to an anti-biotin IgG surface saturation density of 21 ± 2 nmol/m^2 (details in Supporting Information), corresponding to an antibody molecular area of 79 ± 8 nm^2. This molecular area was compared to crystal structure data of an IgG1-subclass mouse-derived antibody.[60] Orienting the antibody structure so that both Fab fragments are directed toward the surface (bivalent binding)[5,12] corresponds to an elliptical area projected onto the surface of 69 nm^2 (Supporting Information, Figure S15). The molecular area determined from the actual IgG surface coverage is 13% greater than the estimate from the crystal structure projection, which may be expected based on differences in packing and conformation of the hydrated surface-bound protein[57] compared to its crystal structure.

Lipid-tethered ligand accessibility in supported-lipid bilayers and monolayers. It has been recently shown that head-group modified phospholipids can exchange between the leaflets of fluid-phase supported-lipid bilayers,[61,62] a process that could impact the population of lipid-tethered ligands available for binding to proteins at the solution-accessible outer-leaflet of a lipid bilayer. The rate of phospholipid translocation between leaflets is sensitive to the phase of the phospholipid bilayer. Unlike the rapid phospholipid translocation observed at liquid-crystalline phase supported bilayers,[16,17,63] gel-phase bilayers well below their respective melting transition temperatures have been shown to exhibit much slower rates of leaflet translocation. Thus, a comparison of protein binding at gel- versus liquid-crystalline-phase bilayers could reveal differences in ligand-tethered lipid translocation. However, differences in the lateral mobility of gel- versus fluid-phase bilayers[64] may also impact ligand accessibility and thereby complicate the interpretation of results. Because phospholipid bilayer phase impacts the kinetics of both inter-leaflet translocation and lateral-diffusion, we characterize the protein association at both gel-phase (DPPC) and liquid-crystalline phase (POPC) *bilayers and monolayers*. Unlike supported-lipid bilayers, supported-lipid monolayers cannot exhibit inter-leaflet translocation and can serve as a control, where variations in ligand accessibility arising from differences in lipid-phase-dependent lateral mobility may be observed independently of inter-leaflet translocation.

To investigate the impact of lipid phase on lipid-tethered ligand accessibility for antibody binding, suspensions of POPC and DPPC were prepared in buffer with varying mol-fractions (0-5 mol%) of biotin-capped DPPE, sonicated to form small vesicles, and then equilibrated with bare and nitrile-derivatized porous silica particles, forming lipid bilayers and monolayers having varying mol% biotin-capped DPPE. Each of these samples was then equilibrated with 300-nM anti-biotin IgG for ~5-hours. Raman spectra from six different particles of each sample were acquired, averaged, and plotted in Figure 4A-D. As observed in all four plots, Raman scattering intensities from IgG vibrational modes (1003, 1243, 1555, 1672 cm^{-1}) increases as a function of biotinylated-lipid mol fraction until they reach a maximum at a biotin-DPPE concentration that produces a saturated surface coverage of antibody.

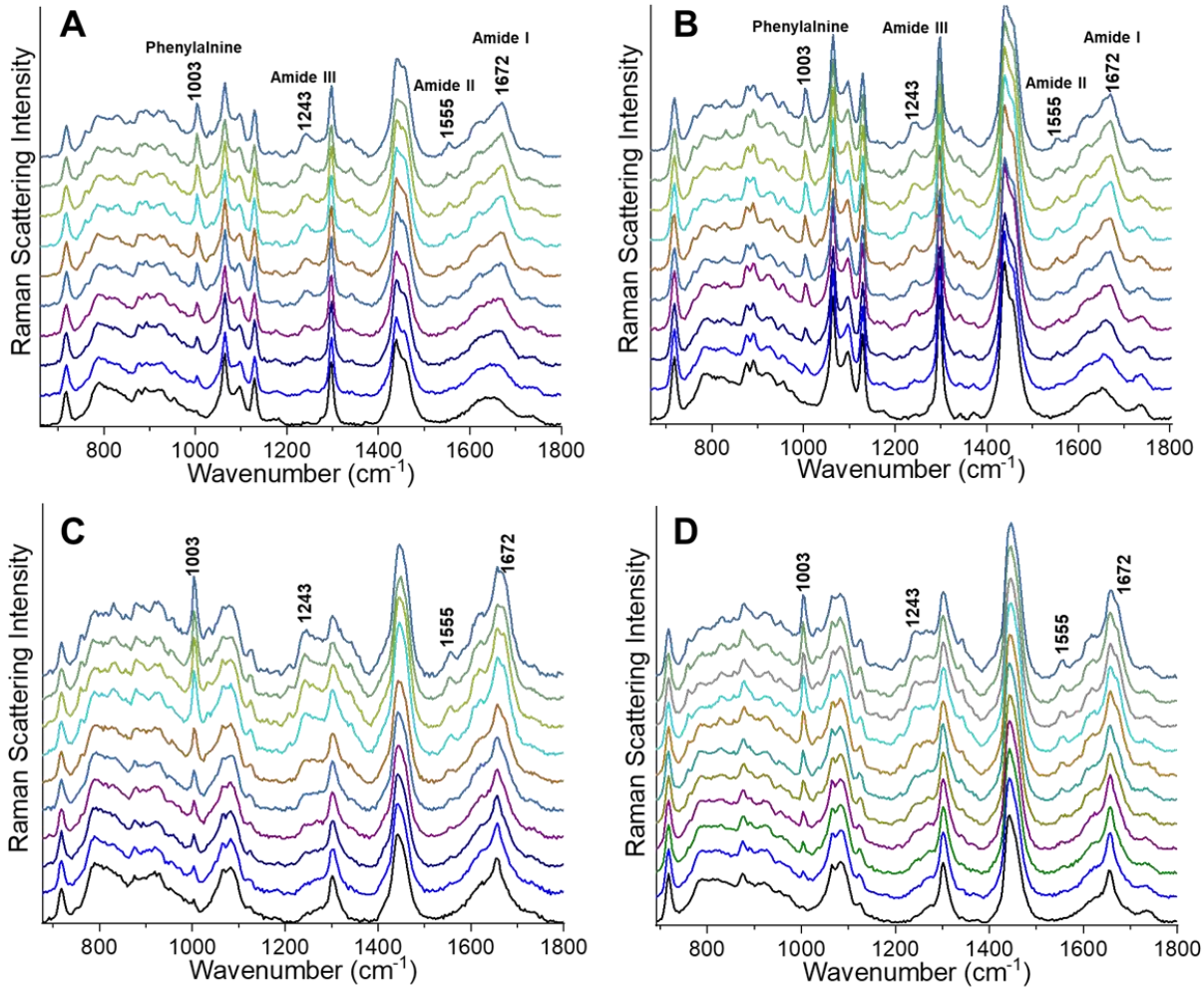

Figure 4. Anti-biotin IgG accumulation as a function of biotin-capped DPPE fraction (0-5 mol%) in a (A) DPPC supported-lipid monolayer, (B) DPPC supported-lipid bilayer, (C) POPC supported-lipid monolayer, and (D) POPC supported-lipid bilayer.

To quantify the accumulated antibody surface coverage, we resolve the anti-biotin IgG Raman spectrum by subtracting the corresponding lipid-bilayer or monolayer spectrum (Figure S16). Using this isolated IgG spectrum, we performed a least-squares fit to determine the relative magnitude of the IgG scattering intensity in each collected spectrum (see examples with residuals in Figures S17-S20) and scaled the result to the maximum coverage determined by elemental carbon analysis. The surface density of biotin-DPPE in each sample was estimated from the mol-fraction of biotinylated lipid times the surface densities of pure POPC and DPPC phospholipid monolayers or distal-leaflet surface densities of their corresponding bilayers (see above). This approach assumes no significant change in average lipid surface density upon substitution of a small fraction (≤ 5-mol%) of biotinylated DPPE for POPC or DPPC in the lipid monolayers or bilayers.

The resulting surface densities of bound-IgG and biotin-DPPE are compared in Figure 5 to evaluate the possible contribution of inter-leaflet translocation to the population of biotin-ligands available for antibody binding in the solution-exposed distal leaflet of a lipid bilayer. An initial observation from these results is that the IgG coverage rises linearly with surface densities of biotin-DPPE in bilayers and monolayers of both DPPC and POPC. The linearity of this relationship indicates that the ratio of IgG bound to the density of available biotin is constant (no change in binding efficiency), until the antibody surface density saturates at high coverages. To report the ratio of IgG surface coverage

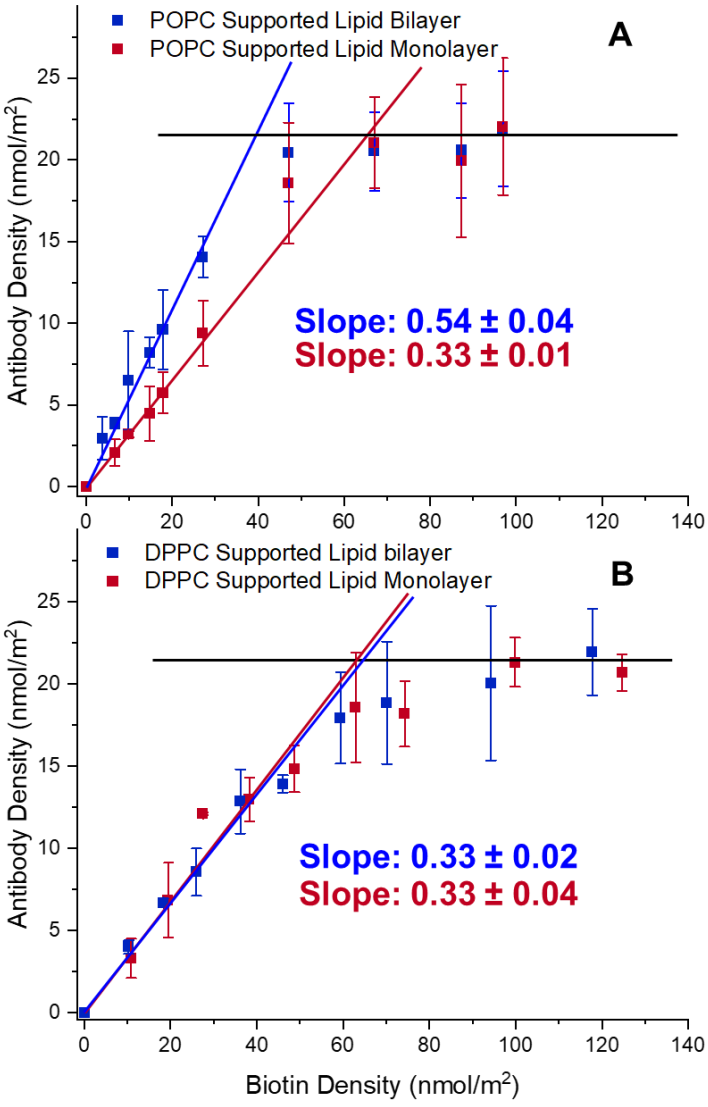

Figure 5. Captured IgG surface density plotted versus biotin-DPPE surface density at a (A) DPPC bilayer (blue) and monolayer (red) and at a (B) POPC bilayer (blue) and monolayer (red). Error bars are 95% confidence bounds. In the case of lipid bilayers, the x-axis is the as-prepared solution-accessible, distal-leaflet biotin density.

to the surface density of biotin available in a lipid monolayer or distal-leaflet of a lipid bilayer, the linear regions (first six points) of all four plots were least-squares fit to a straight line with zero intercept, as shown in Figure 5.

Because gel-phase bilayers well below their melting transition have been shown to exhibit much slower rates of phospholipid translocation between leaflets especially when tethered to a polar molecule,[16] one would anticipate that lipid-leaflet exchange would not contribute significantly to the solution-accessible distal-leaflet population of biotin-DPPE available for IgG binding. This expectation is verified by the equivalent dependence of antibody capture versus biotin-DPPE surface density for *DPPC monolayers and bilayers* (Figure 5A), showing that translocation does not contribute to biotin accessibility at gel-phase bilayer interfaces. The result is consistent with extremely slow rates of lipid translocation at temperatures 20° below the melting transition of DPPC,[16] so that migration of the biotin-DPPE to the distal leaflet of the bilayer does not contribute to the available ligand density over the course of a several-hour IgG accumulation time.

The quantitative nature of these experiments also allows the ratio of the surface density of captured IgG to be compared to the biotin-DPPE ligand density. This ratio is equivalent for capture at both the DPPC monolayer and bilayer, averaging 0.33 ±0.03, the inverse of which indicates that three biotin-DPPE ligands on average are required to capture an anti-biotin antibody. If both variable (Fab) regions of the antibody are bound to biotin ligands (see discussion below), the results would indicate that the efficiency of biotin binding by the antibody at a DPPC bilayer or monolayer surface is ~66%. This inefficiency might arise from slow lateral mobility of lipids in the gel-phase DPPC bilayer or monolayer[64] that could inhibit ligand binding. To test this possibility, the accumulation of anti-biotin IgG by biotin-DPPE dispersed in a *fluid-phase POPC monolayer* was measured, and the results are presented in Figure 5B. The surface density of captured IgG again rises linearly with the surface density of biotin-DPPE, with a slope determined from the first six points that is *equivalent to the gel-phase DPPC monolayer*, 0.33 ±0.01. This result indicates that the IgG capture by biotin-DPPE is independent of the phase of the supporting lipid, so that lipid-phase-dependent differences in lateral mobility play no measurable role in the efficiency of antibody-hapten recognition and binding.

Detecting the influence of lipid translocation on distal-leaflet ligand populations. The equivalent anti-biotin IgG capture efficiency by biotin-DPPE in POPC and DPPC monolayers and DPPC bilayers thus allows the possible influence of inter-leaflet translocation on accessible ligand density to be investigated for fluid-phase POPC bilayers. To examine this question, the IgG surface

coverage is plotted against the as-prepared distal leaflet surface density of biotin-DPPE in a POPC bilayer in Figure 5B, where the slope of the initial linear response (first six points) is determined by a least-squares fit to a straight line with zero intercept. The surface coverage of anti-biotin IgG relative to the as-prepared distal-leaflet biotin surface density exhibits a slope of 0.50 ± 0.03. Neglecting inter-leaflet translocation, this result would indicate that two biotin ligands on the distal leaflet on average are responsible for capturing each anti-biotin IgG, corresponding to bivalent antibody binding. However, this simple interpretation neglects the ligand-binding efficiency revealed by the POPC and DPPC monolayer results, which both showed that three-biotin ligands on average are needed capture to capture a single anti-biotin IgG.

Based on a comparison with the POPC monolayer response in Figure 5B, we attribute the 61 ± 3% greater anti-biotin IgG capture by biotin-DPPE at a POPC bilayer to be a consequence of enhanced ligand density in the distal leaflet through inter-leaflet translocation. It could be hypothesized that this asymmetry might be present at the time the lipid bilayer deposition before exposure to anti-biotin IgG if, for example, there were differences in the affinity of the POPC head-group with the silica surface relative to biotin-DPPE.[21-23] This hypothesis can be rejected, however, because biotin-DPPE in a DPPC bilayer (formed above its melting transition temperature) shows no excess biotin in the distal leaflet of the bilayer. Therefore, the observed asymmetry in the composition of the two leaflets of the POPC bilayer must derive from on-going lipid leaflet exchange of POPC and biotin-DPPE in the fluid-phase bilayer,[16-19] where antibody binding to biotin-DPPE at the solution interface fixes its location in the distal leaflet independent of the biotin-DPPE mol% in the bilayer. This process is analogous to the previous findings where electrostatic interactions of anionic lipids with cationic polyelectrolytes in solution[18,20] or with adsorbed cationic proteins[65] can induce formation of an asymmetric distribution of lipids in the two leaflets of a lipid bilayer. It is clear from these results that inter-leaflet lipid translocation in fluid-phase supported lipid bilayers along with interactions between a lipid-tethered ligand and a solution-phase protein can modify the population of solution-accessible ligands in the distal-leaflet of a supported bilayer, which can confound the interpretation of ligand-density-dependent protein-capture results.

Despite the quantitative capabilities of confocal-Raman microscopy when calibrated by elemental carbon analysis of the samples prepared on high surface area porous supports, the results do not provide direct information on the valency of antibody binding to the biotin ligands on lipid monolayer or bilayer surface. The linear increase in IgG coverage with surface densities of biotin-

DPPE suggests that the valency of antibody binding is constant since it is independent of ligand surface density. With a ratio of three biotin-DPPE ligands per captured IgG, there is clearly sufficient biotin to accommodate bivalent antibody binding. The stability of the captured antibody with no detectable wash-off in 24 hours (Figure S10) would also be consistent with strong and most likely bivalent interactions. If indeed antibody capture is through bivalent binding, that result would suggest that there is sufficient lateral mobility of the biotin-DPPE lipids to allow both Fab fragments to bind to a biotin ligand. While this result would be expected for mobile biotin-DPPE ligands in fluid-phase POPC, the equivalent antibody binding slopes for POPC and DPPC monolayers (Figure 5) suggest that there is sufficient ligand mobility even in the gel-phase DPPC monolayer to provide comparable, likely bivalent, binding. This result is perhaps not surprising because the mobility of gel-phase DPPC lipids in supported-bilayers at 25°C is slow but not zero, where the diffusion coefficient, $D \sim 0.07\ \mu m^2/sec$.[64] At the lowest (0.2%) biotin-DPPE coverage in a DPPC monolayer or bilayer, a two-dimensional random walk predicts that the time for a DPPE-tethered biotin ligand to diffuse the average distance (x~18 nm) separating it from an antibody-bound ligand is $\tau = x^2/4D = 1.2 \times 10^{-3}$ seconds. Thus, the free Fab fragment of a monovalently-bound antibody will encounter a lipid-tethered biotin ligand >800-times per second, even at the lowest biotin-DPPE coverage. These encounters offer many chances for biotin binding compared to the very slow rate of diffusion of unbound antibodies from the surrounding dilute solution into the particle.

Regardless of the valency of antibody binding to biotin ligands, there remains a question about the inefficiency of antibody capture and why an excess of biotin-DPPE on average is required to capture the anti-biotin IgG. Previous studies have suggested that interactions of a lipid-tethered ligand with the surrounding lipid bilayer can interfere with their availability for antibody binding.[10,13] These interactions were evident only in fluid-phase supported bilayers,[13] while in the present case, we observe equivalent ligand-binding efficiency in both fluid- and gel-phase monolayers (Figure 5). Furthermore, while lipid-tethered 2,4-dinitrophenyl (DNP) appeared to interact with fluid-phase POPC and inhibit its antibody binding, lipid-tethered biotin did not.[10] Thus, interactions of biotin with its surrounding lipid bilayer or monolayer do not explain the results. The consistent fraction of biotin ligands that interact with anti-biotin IgG from solution in both fluid-phase or gel-phase monolayers and bilayers may arise from the topology and structure of the porous silica substrate (see Figure S1). There may be regions of inhomogeneous surface structure where a large biomolecule, such as a full-length antibody, is prevented from accessing a

lipid-bound ligand. Geometric constraints that prevent antibody access to some fraction of the surface would be independent of lipid-phase and composition. This issue could perhaps be tested by carrying out experiments using Fab fragments, whose smaller footprint should allow a greater fraction of a supported-lipid monolayer or bilayer surface to be accessible. An additional benefit of these experiments would be that binding valency of the protein would be known, which would provide a quantitative measure of the ligand-binding efficiency.

Conclusions. In this work, we have employed confocal Raman microscopy as a label-free technique to measure the accumulation of proteins as they bind to ligands at supported lipid layers deposited on the interior surfaces of wide-pore silica particles. We carry out direct *in-situ* quantification of monoclonal anti-biotin IgG association with lipid-tethered biotin at POPC and DPPC monolayers and bilayers using Raman spectroscopy calibrated by elemental carbon analysis. At all lipid interfaces studied, the accumulated IgG rises linearly as a function of biotin density until the IgG reaches a saturation coverage. The binding of antibody to gel-phase DPPC bilayers exhibits an identical biotin-coverage response as the accumulation of IgG onto DPPC monolayers. This result contrasts with the behavior of liquid-crystalline POPC bilayers, which exhibit ~60% greater biotin ligands in their distal, solution-accessible leaflet compared to POPC monolayers of the same composition. The additional biotin ligands are likely transferred from the surface-associated proximal leaflet of the bilayer by inter-leaflet translocation, which can be a facile process in liquid-crystalline-phase supported lipid bilayers. The nitrile-supported lipid monolayers used in this investigation were found to be a valuable control substrate to detect the role of inter-leaflet translocation in contributing to solution-accessible ligand densities at supported lipid bilayers. The results suggest caution in interpreting the results of quantitative studies of protein binding to lipid-tethered ligands dispersed in fluid-phase phospholipid bilayers.

ASSOCIATED CONTENT

Supporting Information.

Additional information on nitrile functionalization, quantification of nitrile surface density, formation and quantification of DPPC and POPC monolayers, carbon analysis of POPC bilayer and IgG surface densities, non-specific adsorption controls, reversibility of IgG binding, IgG dimensions from crystallography, determining IgG coverage from Raman spectra, and SEM image of 110-nm pore silica.

ACKNOWLEDGEMENTS

The authors are grateful to Dr. David Parker for acquiring SEM images of the silica particles. This work was supported by the National Science Foundation under Grant CHE-1904424 and from the U.S. Department of Energy, Office of Basic Energy Sciences under Grant DE-FG03-93ER14333. Fellowship support for JPK from the Utah Center for Clinical and Translational Science, funded by the NIH-NLM Training Grant T15 LM00712418, is also acknowledged.

References

(1) Cremer, P.S.; Boxer, S.G. Formation and Spreading of Lipid Bilayers on Planar Glass Supports. *J. Phys. Chem. B* **1999**, *103*, 2554-2559.

(2) Albertorio, F.; Diaz, A.J.; Yang, T.; Chapa, V.A.; Kataoka, S.; Castellana, E.T.; Cremer, P.S. Fluid and Air-Stable Lipopolymer Membranes for Biosensor Applications. *Langmuir* **2005**, *21*, 7476-7482.

(3) Glasmästar, K.; Larsson, C.; Höök, F.; Kasemo, B. Protein Adsorption on Supported Phospholipid Bilayers. *J. Colloid Interface Sci.* **2002**, *246*, 40-47.

(4) Joubert, J.R.; Smith, K.A.; Johnson, E.; Keogh, J.P.; Wysocki, V.H.; Gale, B.K.; Conboy, J.C.; Saavedra, S.S. Stable, Ligand-Doped, Poly(bis-SorbPC) Lipid Bilayer Arrays for Protein Binding and Detection. *ACS Appl. Mater. Interfaces* **2009**, *1*, 1310-1315.

(5) Yang, T.; Baryshnikova, O.K.; Mao, H.; Holden, M.A.; Cremer, P.S. Investigations of Bivalent Antibody Binding on Fluid-Supported Phospholipid Membranes: The Effect of Hapten Density. *J. Am. Chem. Soc.* **2003**, *125*, 4779-4784.

(6) Bryce, D.A.; Kitt, J.P.; Harris, J.M. Confocal Raman Microscopy for Label-Free Detection of Protein–Ligand Binding at Nanopore-Supported Phospholipid Bilayers. *Anal. Chem.* **2018**, *90*, 11509–11516.

(7) Thompson, N.L.; Poglitsch, C.L.; Timbs, M.M.; Pisarchick, M.L. Dynamics of antibodies on planar model membranes. *Acc. Chem. Res.* **1993**, *26*, 567-573.

(8) Tamm, L.K. Lateral diffusion and fluorescence microscope studies on a monoclonal antibody specifically bound to supported phospholipid bilayers. *Biochemistry* **1988**, *27*, 1450-1457.

(9) Müller, K.M.; Arndt, K.M.; Plückthun, A. Model and Simulation of Multivalent Binding to Fixed Ligands. *Anal. Biochem.* **1998**, *261*, 149-158.

(10) Jung, H.; Yang, T.; Lasagna, M.D.; Shi, J.; Reinhart, G.D.; Cremer, P.S. Impact of Hapten Presentation on Antibody Binding at Lipid Membrane Interfaces. *Biophys. J.* **2008**, *94*, 3094-3103.

(11) Jung, H.; Robison, A.D.; Cremer, P.S. Multivalent Ligand-Receptor Binding on Supported Lipid Bilayers. *J. Struct. Biol.* **2009**, *168*, 90-94.

(12) Tamm, L.K.; Bartoldus, I. Antibody binding to lipid model membranes. The large-ligand effect. *Biochemistry* **1988**, *27*, 7453-7458.

(13) Balakrishnan, K.; Mehdi, S.Q.; McConnell, H.M. Availability of Dinitrophenylated Lipid Haptens for Specific Antibody Binding Depends on the Physical Properties of Host Bilayer Membranes. *J. Biol. Chem.* **1982**, *257*, 6434-6439.

(14) Lee, H.J.; Goodrich, T.T.; Corn, R.M. SPR Imaging Measurements of 1-D and 2-D DNA Microarrays Created from Microfluidic Channels on Gold Thin Films. *Anal. Chem.* **2001**, *73*, 5525-5531.

(15) Valles, D.J.; Naeem, Y.; Rozenfeld, A.Y.; Rawan; Wong, A.M.; Carbonell, C.; Mootoo, D.R.; Braunschweig, A.B. Multivalent binding of concanavalin A on variable-density mannoside microarrays. *Faraday Discuss.* **2019**, *219*, 77-89.

(16) Liu, J.; Conboy, J.C. 1,2-Diacyl-Phosphatidylcholine Flip-Flop Measured Directly by Sum-Frequency Vibrational Spectroscopy. *Biophys. J.* **2005**, *89*, 2522-2532.

(17) Gerelli, Y.; Porcar, L.; Lombardi, L.; Fragneto, G. Lipid Exchange and Flip-Flop in Solid Supported Bilayers. *Langmuir* **2013**, *29*, 12762-12769.

(18) Allhusen, J.S.; Conboy, J.C. The Ins and Outs of Lipid Flip-Flop. *Acc. Chem. Res.* **2017**, *50*, 58-65.

(19) Wah, B.; Breidigan, J.M.; Adams, J.; Horbal, P.; Garg, S.; Porcar, L.; Perez-Salas, U. Reconciling differences between lipid transfer in free-standing and solid supported membranes: a time resolved small angle neutron scattering study. *Langmuir* **2017**, *33*, 3384–3394.

(20) Brown, K.L.; Conboy, J.C. Electrostatic Induction of Lipid Asymmetry. *J. Am. Chem. Soc.* **2011**, *133*, 8794-8797.

(21) Stanglmaier, S.; Hertrich, S.; Fritz, K.; Moulin, J.F.; Haese-Seiller, M.; Rädler, J.O.; Nickel, B. Asymmetric Distribution of Anionic Phospholipids in Supported Lipid Bilayers. *Langmuir* **2012**, *28*, 10818-10821.

(22) Doğangün, M.; Hang, M.N.; Troiano, J.M.; McGeachy, A.C.; Melby, E.S.; Pedersen, J.A.; Hamers, R.J.; Geiger, F.M. Alteration of Membrane Compositional Asymmetry by LiCoO2 Nanosheets. *ACS Nano* **2015**, *9*, 8755-8765.

(23) Sun, S.; Liu, C.; Rodriguez Melendez, D.; Yang, T.; Cremer, P.S. Immobilization of Phosphatidylinositides Revealed by Bilayer Leaflet Decoupling. *J. Am. Chem. Soc.* **2020**, *142*, 13003-13010.

(24) Kalb, E.; Engel, J.; Tamm, L.K. Binding of proteins to specific target sites in membranes measured by total internal reflection fluorescence microscopy. *Biochemistry* **1990**, *29*, 1607-1613.

(25) Pisarchick, M.L.; Thompson, N.L. Binding of a monoclonal antibody and its Fab fragment to supported phospholipid monolayers measured by total internal reflection fluorescence microscopy. *Biophys. J.* **1990**, *58*, 1235-1249.

(26) Yang, T.; Jung, S.-Y.; Mao, H.; Cremer, P.S. Fabrication of Phospholipid Bilayer-Coated Microchannels for On-Chip Immunoassays. *Anal. Chem.* **2001**, *73*, 165-169.

(27) Smith, K.A.; Gale, B.K.; Conboy, J.C. Micropatterned Fluid Lipid Bilayer Arrays Created Using a Continuous Flow Microspotter. *Anal. Chem.* **2008**, *80*, 7980-7987.

(28) Smith, E.A.; Thomas, W.D.; Kiessling, L.L.; Corn, R.M. Surface Plasmon Resonance Imaging Studies of Protein-Carbohydrate Interactions. *J. Am. Chem. Soc.* **2003**, *125*, 6140-6148.

(29) Cooper, M.A.; Williams, D.H. Kinetic Analysis of Antibody–Antigen Interactions at a Supported Lipid Monolayer. *Anal. Biochem.* **1999**, *276*, 36-47.

(30) Mack, E.T.; Snyder, P.W.; Perez-Castillejos, R.; Whitesides, G.M. Using Covalent Dimers of Human Carbonic Anhydrase II To Model Bivalency in Immunoglobulins. *J. Am. Chem. Soc.* **2011**, *133*, 11701-11715.

(31) Jung, H.; Robison, A.D.; Cremer, P.S. Detecting Protein−Ligand Binding on Supported Bilayers by Local pH Modulation. *J. Am. Chem. Soc.* **2009**, *131*, 1006-1014.

(32) Nguyen, T.T.; Sly, K.L.; Conboy, J.C. Comparison of the Energetics of Avidin, Streptavidin, NeutrAvidin, and Anti-Biotin Antibody Binding to Biotinylated Lipid Bilayer Examined by Second-Harmonic Generation. *Anal. Chem.* **2012**, *84*, 201-208.

(33) Silverton, E.W.; Navia, M.A.; Davies, D.R. Three-dimensional structure of an intact human immunoglobulin. *Proc. Natl. Acad. Sci. U. S. A.* **1977**, *74*, 5140-5144.

(34) Huber, R.; Deisenhofer, J.; Colman, P.M.; Matsushima, M.; Palm, W. Crystallographic structure studies of an IgG molecule and an Fc fragment. *Nature* **1976**, *264*, 415-420.

(35) Bryce, D.A.; Kitt, J.P.; Harris, J.M. Confocal-Raman Microscopy Characterization of Supported Phospholipid Bilayers Deposited on the Interior Surfaces of Chromatographic Silica. *J. Am. Chem. Soc.* **2018**, *140*, 4071-4078.

(36) Bryce, D.A.; Kitt, J.P.; Myres, G.J.; Harris, J.M. Confocal Raman Microscopy Investigation of Phospholipid Monolayers Deposited on Nitrile-Modified Surfaces in Porous Silica Particles. *Langmuir* **2020**, *36*, 4071-4079.

(37) Maulucci, G.; De Spirito, M.; Arcovito, G.; Boffi, F.; Castellano, A.C.; Briganti, G. Particle Size Distribution in DMPC Vesicles Solutions Undergoing Different Sonication Times. *Biophys. J.* **2005**, *88*, 3545-3550.

(38) Kitt, J.P.; Harris, J.M. Confocal Raman Microscopy for in Situ Detection of Solid-Phase Extraction of Pyrene into Single C18–Silica Particles. *Anal. Chem.* **2014**, *86*, 1719-1725.

(39) Bridges, T.E.; Houlne, M.P.; Harris, J.M. Spatially Resolved Analysis of Small Particles by Confocal Raman Microscopy: Depth Profiling and Optical Trapping. *Anal. Chem.* **2004**, *76*, 576-584.

(40) Brandt, N.N.; Brovko, O.O.; Chikishev, A.Y.; Paraschuk, O.D. Optimization of the Rolling-Circle Filter for Raman Background Subtraction. *Appl. Spectrosc.* **2006**, *60*, 288-293.

(41) Orendorff, C.J.; Ducey, M.W.; Pemberton, J.E. Quantitative Correlation of Raman Spectral Indicators in Determining Conformational Order in Alkyl Chains. *J. Phys. Chem. A* **2002**, *106*, 6991-6998.

(42) Fox, C.B.; Uibel, R.H.; Harris, J.M. Detecting Phase Transitions in Phosphatidylcholine Vesicles by Raman Microscopy and Self-Modeling Curve Resolution. *J. Phys. Chem. B* **2007**, *111*, 11428-11436.

(43) Schultz, Z.D.; Levin, I.W. Vibrational Spectroscopy of Biomembranes. *Annu. Rev. Anal. Chem.* **2011**, *4*, 343-366.

(44) Czamara, K.; Majzner, K.; Pacia, M.Z.; Kochan, K.; Kaczor, A.; Baranska, M. Raman spectroscopy of lipids: a review. *J. Raman Spectrosc.* **2015**, *46*, 4-20.

(45) Levin, I.W. Vibrational spectroscopy of membrane assemblies. *Adv Infrared Raman Spec* **1984**, *11*, 1-48.

(46) Rowlen, K.L.; Harris, J.M. Raman spectroscopic study of solvation structure in acetonitrile/water mixtures. *Anal. Chem.* **1991**, *63*, 964-969.

(47) White, R.J.; Ervin, E.N.; Yang, T.; Chen, X.; Daniel, S.; Cremer, P.S.; White, H.S. Single Ion-Channel Recordings Using Glass Nanopore Membranes. *J. Am. Chem. Soc.* **2007**, *129*, 11766-11775.

(48) Schibel, A.E.P.; Edwards, T.; Kawano, R.; Lan, W.; White, H.S. Quartz Nanopore Membranes for Suspended Bilayer Ion Channel Recordings. *Anal. Chem.* **2010**, *82*, 7259-7266.

(49) Kitt, J.P.; Harris, J.M. Confocal Raman Microscopy of Hybrid-Supported Phospholipid Bilayers within Individual C18-Functionalized Chromatographic Particles. *Langmuir* **2016**, *32*, 9033-9044.

(50) Janiak, M.J.; Small, D.M.; Shipley, G.G. Temperature and compositional dependence of the structure of hydrated dimyristoyl lecithin. *J. Biol. Chem.* **1979**, *254*, 6068-6078.

(51) Akutsu, H. Direct determination by Raman scattering of the conformation of the choline group in phospholipid bilayers. *Biochemistry* **1981**, *20*, 7359-7366.

(52) Nagle, J.F.; Tristram-Nagle, S. Structure of lipid bilayers. *Biochim. Biophys. Acta, Rev. Biomembr.* **2000**, *1469*, 159-195.

(53) Kučerka, N.; Tristram-Nagle, S.; Nagle, J.F. Closer Look at Structure of Fully Hydrated Fluid Phase DPPC Bilayers. *Biophys. J.* **2006**, *90*, L83-L85.

(54) Rygula, A.; Majzner, K.; Marzec, K.M.; Kaczor, A.; Pilarczyk, M.; Baranska, M. Raman spectroscopy of proteins: a review. *J. Raman Spectrosc.* **2013**, *44*, 1061-1076.

(55) San Paulo, A.; García, R. High-Resolution Imaging of Antibodies by Tapping-Mode Atomic Force Microscopy: Attractive and Repulsive Tip-Sample Interaction Regimes. *Biophys. J.* **2000**, *78*, 1599-1605.

(56) Zhang, P.C.; Bai, C.; Ho, P.K.H.; Dai, Y.; Wu, Y.S. Observing interactions between the IgG antigen and anti-IgG antibody with AFM. *IEEE Eng. Med. Biol. Mag.* **1997**, *16*, 42-46.

(57) Leatherbarrow, R.J.; Stedman, M.; Wells, T.N.C. Structure of immunoglobulin G by scanning tunnelling microscopy. *J. Mol. Biol.* **1991**, *221*, 361-365.

(58) Chen, Y.; Cai, J.; Xu, Q.; Chen, Z.W. Atomic force bio-analytics of polymerization and aggregation of phycoerythrin-conjugated immunoglobulin G molecules. *Mol. Immunol.* **2004**, *41*, 1247-1252.

(59) Harris, L.J.; Larson, S.B.; Hasel, K.W.; McPherson, A. Refined Structure of an Intact IgG2a Monoclonal Antibody. *Biochemistry* **1997**, *36*, 1581-1597.

(60) Harris, L.J.; Skaletsky, E.; McPherson, A. Crystallographic structure of an intact IgG1 monoclonal antibody. *J. Mol. Biol.* **1998**, *275*, 861-872.

(61) Jing, Y.; Kunze, A.; Svedhem, S. Phase Transition-Controlled Flip-Flop in Asymmetric Lipid Membranes. *J. Phys. Chem. B* **2014**, *118*, 2389-2395.

(62) Jing, Y.; Trefná, H.D.; Persson, M.; Svedhem, S. Heat-activated liposome targeting to streptavidin-coated surfaces. *Biochim. Biophys. Acta* **2015**, *1848*, 1417-1423.

(63) Schoch, R.L.; Barel, I.; Brown, F.L.H.; Haran, G. Lipid diffusion in the distal and proximal leaflets of supported lipid bilayer membranes studied by single particle tracking. *J. Chem. Phys.* **2018**, *148*, 123333.

(64) Scomparin, C.; Lecuyer, S.; Ferreira, M.; Charitat, T.; Tinland, B. Diffusion in supported lipid bilayers: Influence of substrate and preparation technique on the internal dynamics. *Eur. Phys. J. E: Soft Matter Biol. Phys.* **2009**, *28*, 211-220.

(65) Luo, J.-J.; Wu, F.-G.; Qin, S.-S.; Yu, Z.-W. In Situ Unfolded Lysozyme Induces the Lipid Lateral Redistribution of a Mixed Lipid Model Membrane. *J. Phys. Chem. B* **2012**, *116*, 12381-12388.

TOC GRAPHIC